AIAA SciTech Forum
9 - 13 January 2017, Grapevine, Texas
55th AIAA Aerospace Sciences Meeting
AIAA 2017-0230

The Very Near Pressure Field of Single- and Multi-Stream Jets

Dimitri Papamoschou* and Vincent Phong †
University of California, Irvine, Irvine, CA, 92697, USA

We present experimental data towards the development of a low-order model for the jet noise source for predictions of isolated and installed noise. In the proposed scheme, the source is prescribed on a radiator surface defining the boundary between the inner rotational jet flow and the outer linear pressure field. The source consists of wavepacket-type partial fields whose noise emission can be computed using well-established linear propagation methods. Experiments on single- and dual-stream jets are used to define the radiator surface and determine relevant quantities on it, including the convective velocity, axial correlation scale, and azimuthal coherence. It is found that the rotational/irrotational boundary is characterized by negative skewness of the pressure field, leading to a convenient criterion for defining the radiator surface. Space-time correlations of the pressure fluctuation on the radiator surface yield the distribution of convective velocity U_c of the partial fields. In coaxial jets, the outer flow effectively silences the eddies of the primary shear layer in the vicinity of the nozzle exit. This is manifested by a large drop of U_c in the initial region of the jet. Offsetting the nozzles prolongs the low-U_c region on the side of the thickened secondary flow. The resulting reduction in radiation efficiency is deemed the primary reason for the noise benefit of eccentric jets. Circumferential coherence measurements indicate that the partial fields are very localized azimuthally.

I. Introduction

Noise emission has become a prominent consideration in the design of aircraft and their propulsion systems. This is driven by the need for community noise compliance and reduction of the exposure of military personnel to unhealthy sound pressure levels. The integrated nature of aircraft design requires system-level approaches to noise prediction and noise reduction, using tools that can generate high-fidelity answers in a matter of hours or minutes. The sources of noise (e.g., turbulent jets, rotor-stator interactions) involve fluid-mechanical processes that are very complex, not fully understood, and still the subject of fundamental investigations. The interaction of the emitted sound with solid and fluid surfaces associated with the aircraft and its propulsion must also be accounted for in the system-level noise prediction. Even though highly resolved fluid dynamics solutions are possible through advances in large eddy simulation (LES) and related methods, the large computational cost and long turnaround times make these approaches unfeasible for design purposes. There is a need for simplified physical models of the noise sources, informed by low-cost computations, that can be coupled with efficient propagation schemes.

The simplification, however, must retain the stochastic nature of the noise sources. Jet noise, broadband fan noise, and airframe noise are examples of sources associated with turbulence and

*Professor, Department of Mechanical and Aerospace Engineering, Fellow AIAA
†Assistant Specialist, Department of Mechanical and Aerospace Engineering, Member AIAA

therefore are stochastic. This clearly poses a challenge with the propagation step because propagation techniques treat deterministic fields. This challenge can be overcome by describing the stochastic source in terms of a number of deterministic *partial fields* whose parameters follow certain distributions. The total propagated field would be synthesized from the individual propagated fields based on the probability density functions of the source parameters. It is desired to inform the partial fields by low-cost computations, such as Reynolds-Averaged Navier Stokes (RANS) flow field solutions.

For the jet noise source, the topic of this paper, the proposed predictive scheme is presented at a simplified level in Fig. 1. The partial fields are prescribed on a conical-shaped "radiator surface" at the boundary between the inner nonlinear rotational flow field and outer linear pressure field. It is on this surface that the linear pressure distribution reflects the "footprint" of the turbulence, and in particular the coherent structures that dominate mixing and noise generation.[1,2] As we move outward from this surface, the hydrodynamic information is rapidly filtered out and the footprint is lost. Thus, any attempt of linking the structure of the linear pressure field to the structure of the underlying turbulence field must be done on this radiator surface. Once the noise source on the radiator surface is properly modeled, propagation to an observer outside the surface would involve well established linear tools, such as the boundary element method.

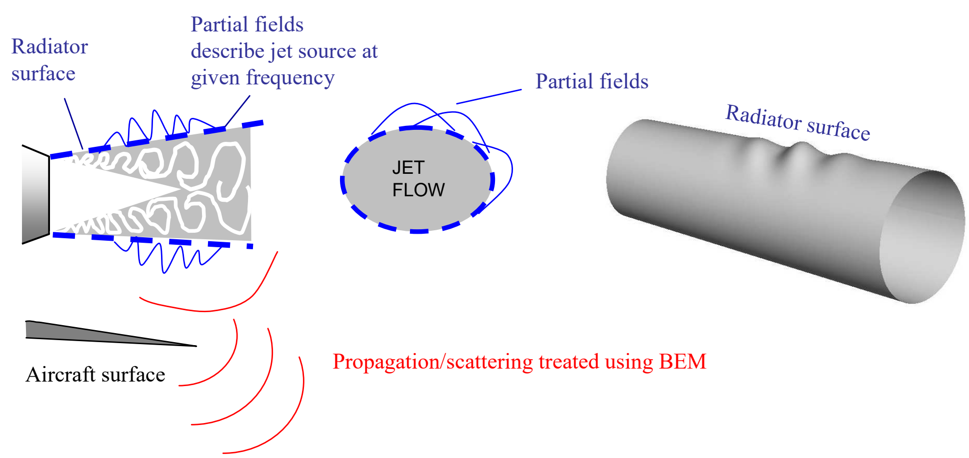

Figure 1. Basic elements of predictive scheme for jet noise and its interactions.

The partial fields are defined in terms of the pressure fluctuation p' on the radiator surface. For a given frequency, each partial field is envisioned to be an amplitude modulated traveling wave with finite axial and azimuthal scales, reflecting the wavepacket nature of jet noise that has been the subject of numerous studies.[3–8] Certain elements of the partial field (e.g., its position and amplitude) would be random, while others would be deterministic. Among the most critical parameters of the partial field is its convective velocity U_c, which is expected to be influenced by the convective velocity of the underlying coherent structures in the jet flow. The convective Mach number $M_c = U_c/a$, where a is the ambient speed of sound, governs the radiation efficiency of high-speed jets and its reduction can lead to significant noise suppression.[9]

The proposed prediction method requires computational and experimental knowledge of the salient statistics on the radiator surface. The present paper is a continuation of earlier computational studies of the statistics on the radiator surface of a single-stream jet and the connection to the RANS solution.[10] Here we examine experimentally the very near pressure field of dual-stream jets, with emphasis on understanding the principal mechanisms behind the noise reduction measured in "offset-stream" jets.[11–14] Results from one of the early studies of offset-stream jets, Ref.

15, are shown in Fig. 2. At that time, it was speculated that the reduction in noise emission of the eccentric jet was due to the reduction of the convective Mach number.[15,16] The arguments were based on simplified models for the mean flow field and lacked direct evidence. The present study provides information that supports those early conjectures with detailed measurements of the statistics in the very near pressure fields of coaxial and eccentric jets.

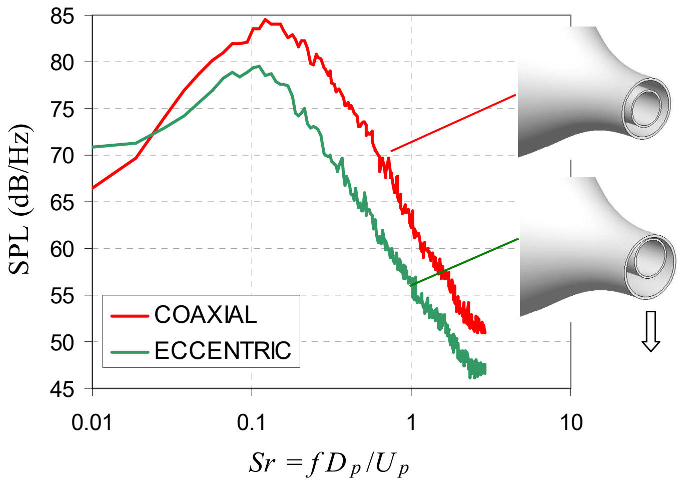

Figure 2. Spectra in the direction of peak emission for coaxial and eccentric jets with primary velocity of 600 m/s, secondary velocity of 400 m/s, and bypass ratio of 2.5. From Ref.15.

II. Radiator Surface

Any surface surrounding the jet that does not include the vortical field can be used as a "source surface" to propagate outward and compute the sound field. That surface would have a particular distribution of U_c, depending on its shape (e.g., cone, cylinder, etc), and its distance from the jet axis. However, there is only one such surface that contains the full hydrodynamic component of the pressure field, that is, the signature of the turbulent motion of the eddies inside the jet. This surface is the edge of the jet, defined here as the closest surface to the jet centerline on and outside of which the propagation of pressure perturbation is governed by the homogeneous linear wave equation. If a connection is to be made between a fluid-mechanical velocity and a convective velocity in the linear pressure field, the latter would need to be defined on the edge surface. Outside the edge surface, the hydrodynamic information is lost quickly.

Following the analysis of Papamoschou *et al.*,[10] the criterion for the location of the radiator surface can be formed as

$$\frac{d\overline{u}/dr}{(d\overline{u}/dr)_{max}} \to 0 \tag{1}$$

where $\overline{u}$ is the mean axial velocity and r is the radial coordinate. Accordingly, the edge $r_{edge}(x)$ is defined as the radial position where the radial gradient of the mean axial velocity, normalized by its local peak value, equals a given threshold $\kappa << 1$:

$$\frac{|d\overline{u}/dr|(x, r_{edge}(x))}{|d\overline{u}/dr|_{max}(x)} \;=\; \kappa \tag{2}$$

The threshold selected here is $\kappa = 0.01$. However, the accurate determination of the mean velocity gradient at the edge of the jet is very difficult experimentally because probes lose resolution in the low-speed region of the jet. Therefore, the criterion of Eq. 2 can be impractical. Alternate means of identifying this location are desirable.

III. Experimental Setup

The experiment utilized single- and dual-stream cold air jets in the UCI Jet Aeroacoustics facility. In the single-stream experiments, the jet was issued from a convergent round nozzle with inner diameter $D_p = 14.2$ mm and lip thickness of 0.51 mm. For the dual-stream investigations, an outer round nozzle with inner diameter $D_s = 23.4$ mm was installed around the primary nozzle. The exits of the inner and outer nozzles were co-planar. Figure 3 shows the coordinates and a photo of the nozzles. Coaxial and eccentric configurations were tested via transverse translation of the inner nozzle relative to the outer nozzle. In all the experiments reported here, the primary flow was at Mach number $M_p = 0.9$ and velocity $U_p = 286$ m/s. The velocity ratio of the secondary flow took the values $U_s/U_p = 0.5$ and 0.7. The latter value is representative of core-bypass velocity ratios in modern turbofan engines. The Reynolds number of the primary jet was 3.6×10^5.

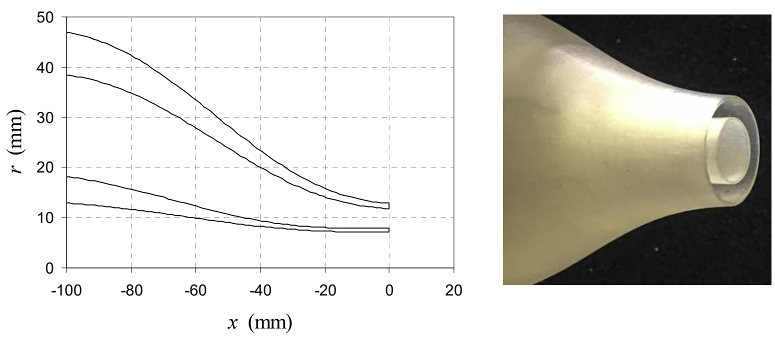

Figure 3. Radial coordinates and photo of coaxial nozzle.

Diagnostics included Pitot measurements of the mean velocity field and time-resolved measurements of the pressure in the near field of the jets. Of particular interest was the pressure field on or near the radiator surface defined in the previous section. Given the proximity of this surface to the rotational flow field, conventional microphones can easily be destroyed by contact with the flow. Instead, piezoresistive pressure transducers were used as substitutes for microphones. The experiment employed five Endevco Model 8507C-15 transducers with probe diameter of 2.42 mm and dynamic range of 0-15 psig. The transducers have a resonance frequency of 130 kHz, about one third of which (43 kHz) defines the upper limit of their range. They were sampled simultaneously at a rate of 250 kS/s, and their output was filtered digitally using a four-pole Butterworth filter with 30 kHz frequency cutoff. The transducers are mounted inside holders that have the external shape of the Bruel & Kjaer Model 4138 microphone and pre-amplifier; thus they are interchangeable with the microphones in the various array deployments.

Results in the frequency domain will be presented in terms of the Strouhal number based on the primary flow variables

$$Sr = \frac{fD_p}{U_p} = \frac{\omega D_p}{2\pi\, U_p}$$

where f is the cyclic frequency and ω is the radian frequency. The frequency cutoff restricted the upper limit of the Strouhal number to 1.5.

The transducers were deployed in axial and azimuthal arrays exemplified in Figs. 4 and 5, respectively. In the axial deployment, the probes were uniformly spaced apart by 7.94 mm and the probe tips were aligned along the radiator surface. In the azimuthal deployment, the transducers were mounted at uneven azimuthal separations $\Delta\phi$ so that their permutations resulted in adequate coverage of the azimuthal separation angle. The microphone holders have elongated triangular cross sections, with the sharp end pointing towards the source, to minimize reflections from the holder toward the microphone.

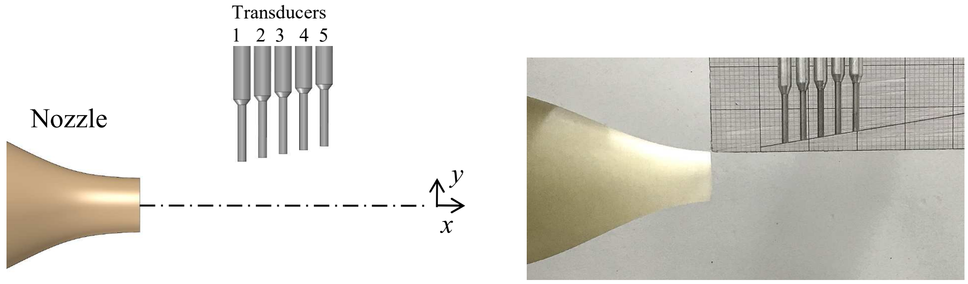

Figure 4. Layout of axial probe array.

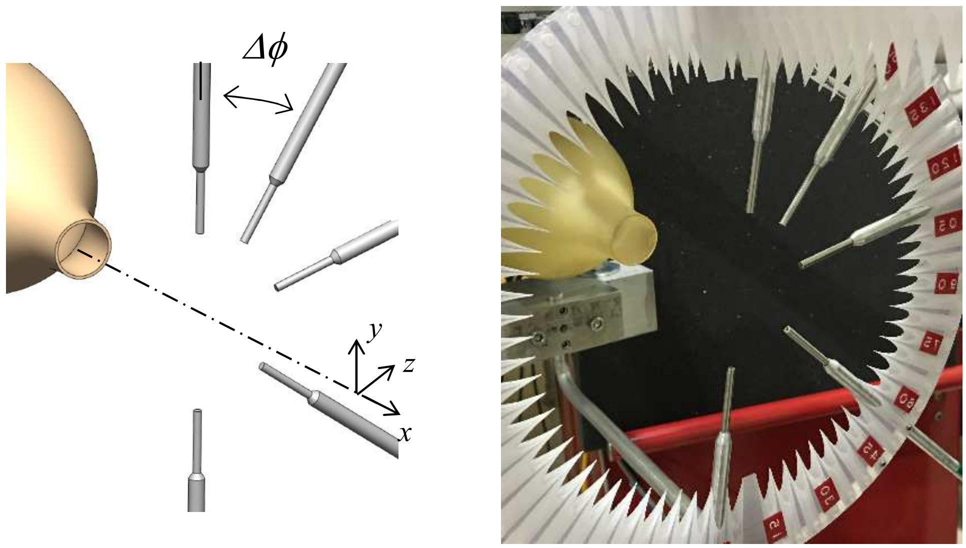

Figure 5. Layout of azimuthal probe array.

IV. Results

A. Mean Velocity Field

Figure 6 shows contour plots of the mean axial velocity field of the single, coaxial, and eccentric jets. The dual-stream jets were issued at $U_s/U_p = 0.7$. The salient flow features of the axisymmetric jets have been discussed in past works[17] but are included here for completeness. The length of the primary potential core L_p is defined here as the axial distance from the nozzle exit where the centerline velocity drops to 90 % of the primary exit velocity. For the single-stream jet, $L_p/D_p = 8$. Addition of the coaxial secondary flow stretches the potential core length to $L_p/D_p = 12$. For the eccentric configurations, the potential core elongates only slightly, to $L_p/D_p = 9$, relative to the single-stream case. This indicates enhanced mixing of the eccentric jet, occurring on the thin side of the secondary flow, relative to the coaxial case. From the data of Fig. 6, combined with past studies of these flows, the secondary potential core length is $L_s/D_p = 4$ for the coaxial jet and $L_s/D_p = 7$ for the underside of the eccentric jet. In other words, for the eccentric jet the secondary and primary potential cores have similar lengths on the thick side of the secondary flow.

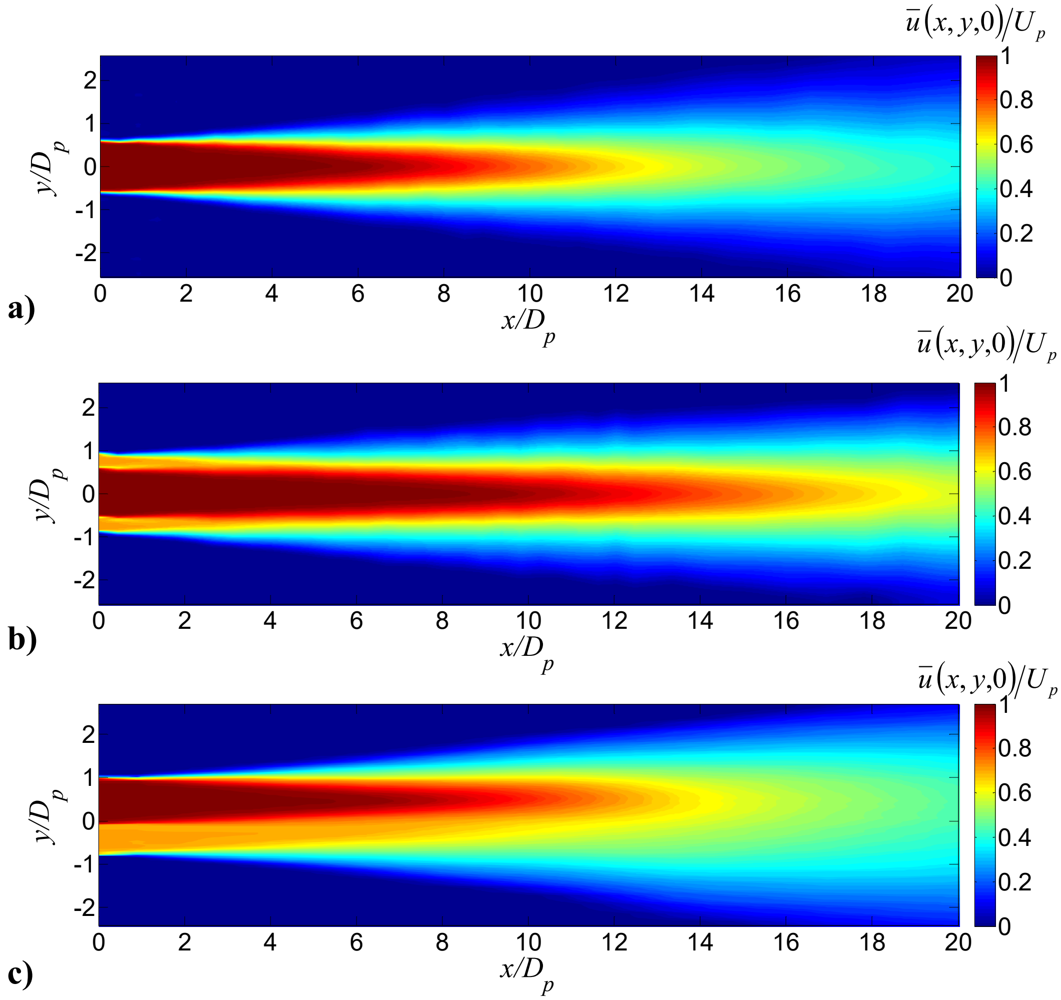

Figure 6. Contours of mean axial velocity for: a) single-stream jet; b) coaxial jet; and c) eccentric jet.

B. Skewness Criterion for Radiator Surface

In an attempt to establish a more practical methodology for defining the radiator surface than the gradient criterion of Eq. 2, the statistics of the pressure field were examined in both LES[10] and in the current experiments. Considering the normalized skewness

$$Sk = \frac{< p'^3 >}{(< p'^2 >)^{3/2}} \tag{3}$$

where <> denotes the time average, an interesting trend was observed in both sets of data: the skewness forms a negative layer at the edge of the jet. See Fig. 7(a). The criterion

$$Sk = -0.3$$

was found to consistently give the same location as the gradient criterion of Eq. 2, with $\kappa = 0.01$. The same observation applies to the LES data of Ref. 10. Figure 7(b) compares the two criteria for the single-stream Mach 0.9 jet, where it is shown that they practically coincide. Although the physical reasons for this overlap, and the existence of the negative skewness layer, remain under investigation, the $Sk = -0.3$ criterion constitutes a practical detection scheme that can obviate the mean flow survey of the jet and the challenging calculation of the mean velocity gradient.

The $Sk = -0.3$ criterion was also used to define the radiator surface of the coaxial jet at $U_s/U_p = 0.7$. Because the procedure is still laborious, the radiator surface of the coaxial jet with $U_s/U_p = 0.5$ was assumed to be very close to that of the jet with $U_s/U_p = 0.7$. Similarly, the eccentric jets utilized the radiator surface of the coaxial jet at $U_s/U_p = 0.7$. Judging from the mean flow profiles of Fig. 6, this is a good approximation on the symmetry plane up to about $x/D_p = 12$. However, off the symmetry plane the edges of the coaxial and eccentric jets can be different, and this should be kept in mind when examining some of the results that follow.

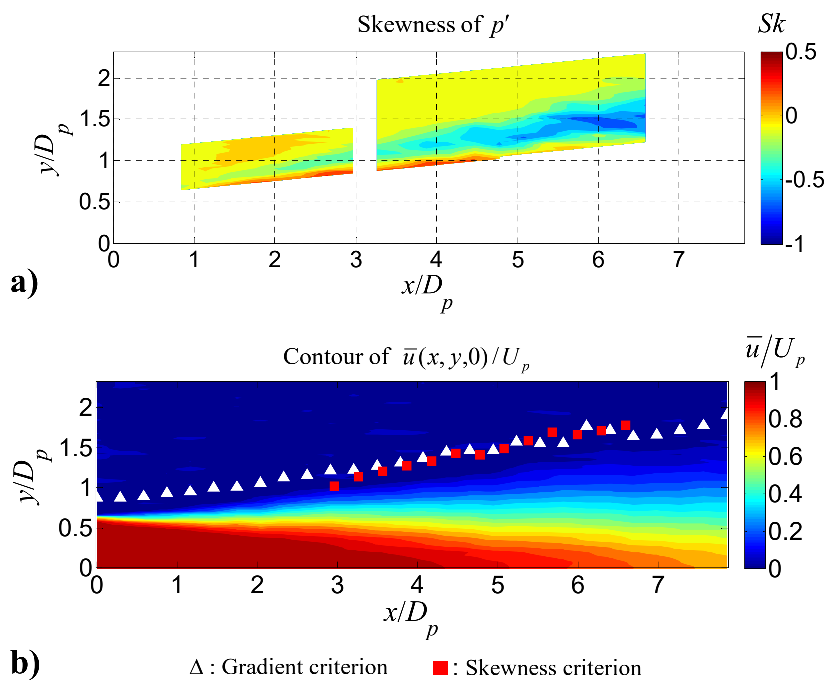

Figure 7. Definition of the radiator surface for the single-stream jet. (a) Experimental contours of pressure skewness near the edge of the jet; (b) mean velocity field, with comparison of the gradient and skewness criteria for the location of the radiator surface.

C. Axial Space-Time Correlations

The probe outputs of the axial array were processed to obtain the space-time correlation of the pressure fluctuation on the radiator surface

$$R_{pp}(x;\xi,\tau) \quad = < p'(x,t)\; p'(x+\xi,t+\tau) > \tag{4}$$

where ξ is the axial separation, τ is the time separation, and $<>$ denotes the time average. The normalized space-time correlation is defined as

$$\widetilde{R}_{pp}(x;\xi,\tau) \quad = \frac{R_{pp}(x;\xi,\tau)}{R_{pp}(x;0,0)} \tag{5}$$

Figure 8 plots representative space-time correlations for single-stream and dual-stream coaxial jets. The trends are similar to those of space-time correlations measured inside the jet flow field,[18,19] although the negative loops are more prominent here.

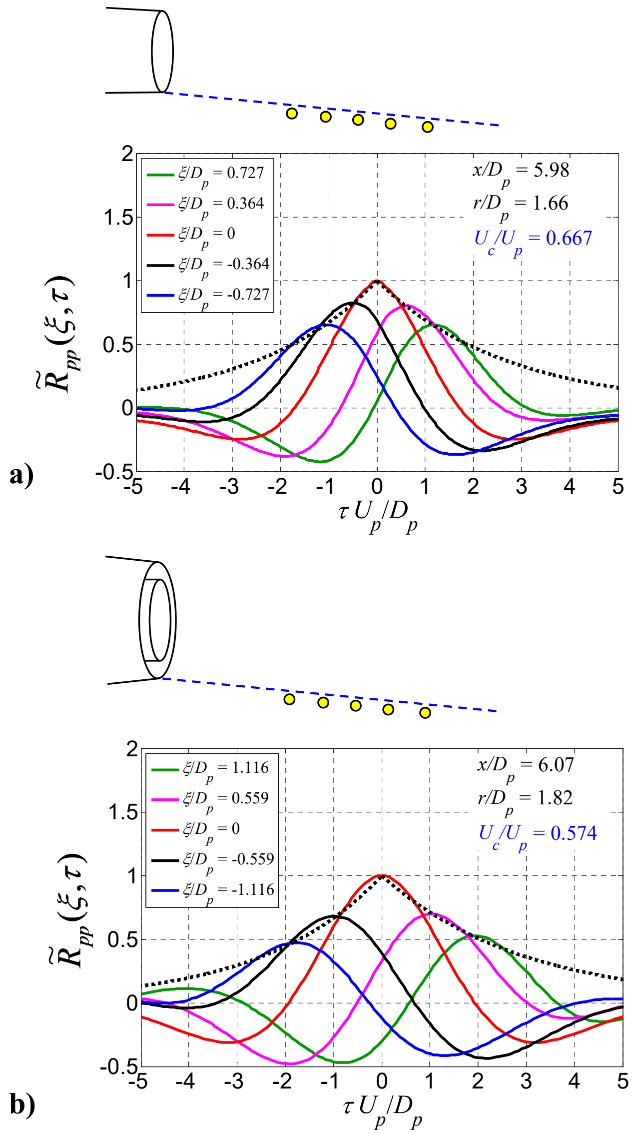

Figure 8. Examples of axial space-time correlations at $x/D_p = 6$ on the respective radiator surfaces for: a) single-stream jet; and b) coaxial jet. Dashed lines indicate the spatial decay envelopes.

The convective velocity was computed using the middle (third) probe of the axial array of Fig. 4 as reference. Denoting the reference location as x_0, computation of the convective velocity at x_0 involved the space-time correlations at $\xi_i = x_i - x_0$, $i = -2, -1, 1, 2$, where x_i are the locations of the surrounding probes. Because each correlation function comprises a discrete set of points, to accurately locate the maximum value of the correlation a seventh-order polynomial was fitted around the peak of the correlation curve. The time separation corresponding to the maximum value of the polynomial (i.e., the root of the derivative), τ_i, was then calculated using a Newton-Raphson iteration method. The convective velocity was obtained from

$$U_c(x_0) \;=\; \frac{1}{4} \sum_{i=-2,-1,1,2} \frac{\xi_i}{\tau_i} \tag{6}$$

D. Convective Velocity Distributions

In all the results that follow, the convective velocity will be presented in the non-dimensional form U_c/U_p. Figure 9 plots the axial distributions of U_c/U_p for all the axisymmetric jets of this study, including the single-stream jet, on their respective radiator surfaces. For the single-stream jet, the convective velocity is fairly constant over the extent of the measurement region $0 \leq x/D_p \leq 10$, averaging to about $U_c/U_p = 0.62$. This is consistent with past LES results on the radiator surface of the single-stream jet.[10] For the jets issuing from the coaxial nozzle, the radiator surface was defined by the skewness criterion $Sk = -0.3$ applied to the jet with $U_s/U_p = 0.7$. The coaxial case with $U_s/U_p = 0$ represents again the single-stream jet, but now the radiator surface is placed outward at the location of the jet with $U_s/U_p = 0.7$. On this radiator surface and within the axial extent of the potential core, U_c/U_p is about 10 % higher than on the inner radiator surface. This could be the result of the conversion of the hydrodynamic field into the faster-propagating acoustic field.[10] The convective velocity declines rapidly past $x/D_p = 10$. Focusing now on the cases with secondary flow, we note a dramatic drop of U_c/U_p in the first few jet diameters. This indicates that the primary shear layer becomes "silent" there and U_c on the radiator surface is dominated by the convection of the eddies in the secondary shear layer. On the other hand, far from the nozzle exit convective velocity returns to values around $U_c/U_p = 0.65$. These values are associated with the elongation of the primary potential core with application of the secondary flow.[17]

Considering the eccentric jets, Fig. 10 plots the convective velocity distribution on the thick and thin sides of the secondary flow, and compares to the corresponding coaxial cases, for U_s/U_p=0.5 and 0.7. The dramatic reduction of U_c/U_p on the thick side of the eccentric jets is due to the elongation of the secondary potential core, evident in Fig. 6(c), coupled with compaction of the primary potential core. As a result, the convective velocity starts at low level and reduces past $x/D_p \approx 6$ as the mean flow velocity decays. On the thin side, the convective velocity starts at levels similar to those of the single-stream jet ($U_c/U_p \approx 0.6$), then declines rapidly past $x/D_p = 5$.

The reduction in convective velocity on the thick side of the eccentric jets, and attendant reduction in radiation efficiency,[9] explains the noise suppression characteristics of offset-stream jets. The results of Figs. 10 constitute the first direct evidence of this important noise suppression mechanism.

E. Axial Correlation Scale

The envelope of the space-time correlations, shown by dashed lines in the space-time correlations of Fig. 8, provides a means to estimate the axial correlation length scale $L_x(x)$. The envelope connects the peaks of the individual correlation curves and is assumed here to have the the exponential form

$$R_x(x;\xi) \;=\; \exp\left(-\left|\frac{\xi}{L_x(x)}\right|\right) \tag{7}$$

However, Eq. 7 does not fully capture the non-stationarity of the statistics in x. As is evident from the plots of Fig. 8, the space-time correlation is not symmetric around $\tau = 0$ and thus is not symmetric around $\xi = 0$. Because of this, we resort to the compound relation

$$\begin{aligned} R_x(x;\xi \geq 0) \;&=\; \exp\left(-\left|\frac{\xi}{L_{x,\mathrm{right}}(x)}\right|\right) \\ R_x(x;\xi \leq 0) \;&=\; \exp\left(-\left|\frac{\xi}{L_{x,\mathrm{left}}(x)}\right|\right) \end{aligned} \tag{8}$$

and use the average value

$$L_x(x) \;=\; \frac{1}{2}\left(L_{x,\mathrm{left}}(x) + L_{x,\mathrm{right}}(x)\right) \tag{9}$$

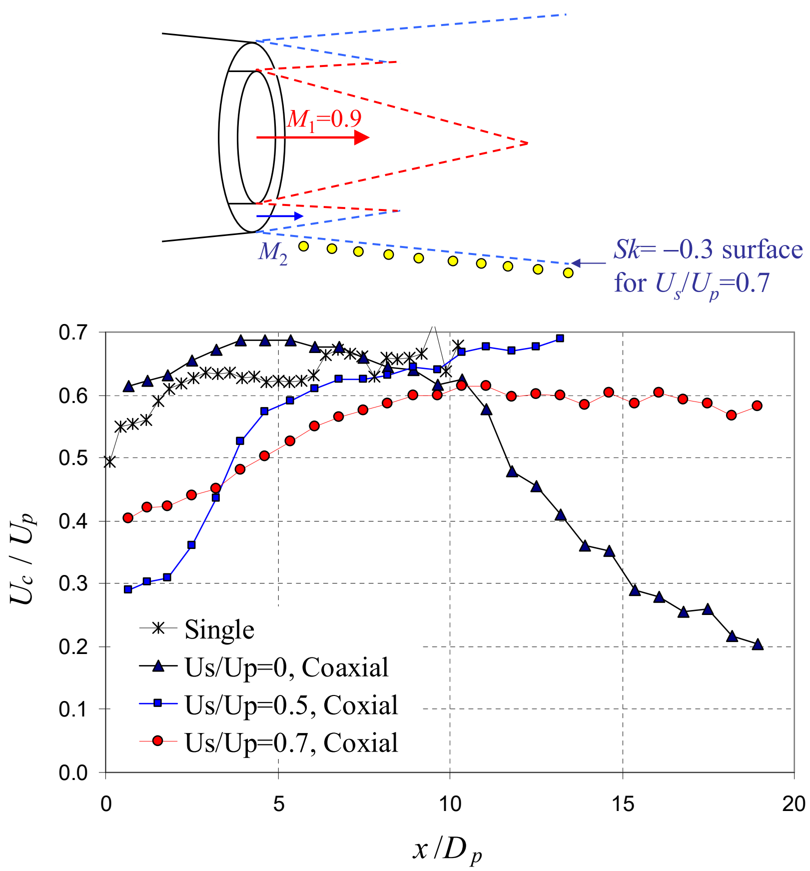

Figure 9. Convective velocity distribution in axisymmetric jets.

as the axial correlation scale. The length scales $L_{x,\text{left}}$ and $L_{x,\text{right}}$ were determined by least-squares fits of Eq. 8 to the space-time correlation data.

Figure 11 plots the axial distributions of L_x for the single-stream jet, and coaxial and eccentric jets with $U_s/U_p = 0.7$. For the single-stream jet, L_x follows a linear trend with x and its value at the end of the potential core is $L_x \approx 2D_p$. For the coaxial jet, there is an initial bump associated with the secondary shear layer, followed by a linear trend. Near the end of the primary potential core, $L_x \approx 3D_p$. On the thick side of the eccentric jet, there is an initial bump similar to that of the coaxial jet; however, L_x then declines to a fairly constant value of $L_x/D_p \approx 1$. On the thin side of the eccentric jet, L_x overlaps with that of the single stream jet for the first five diameters, then grows at a very weak rate. Overall, the eccentric jet shows a surprising level of decorrelation, which could be a contributing factor to the its reduced noise emission.

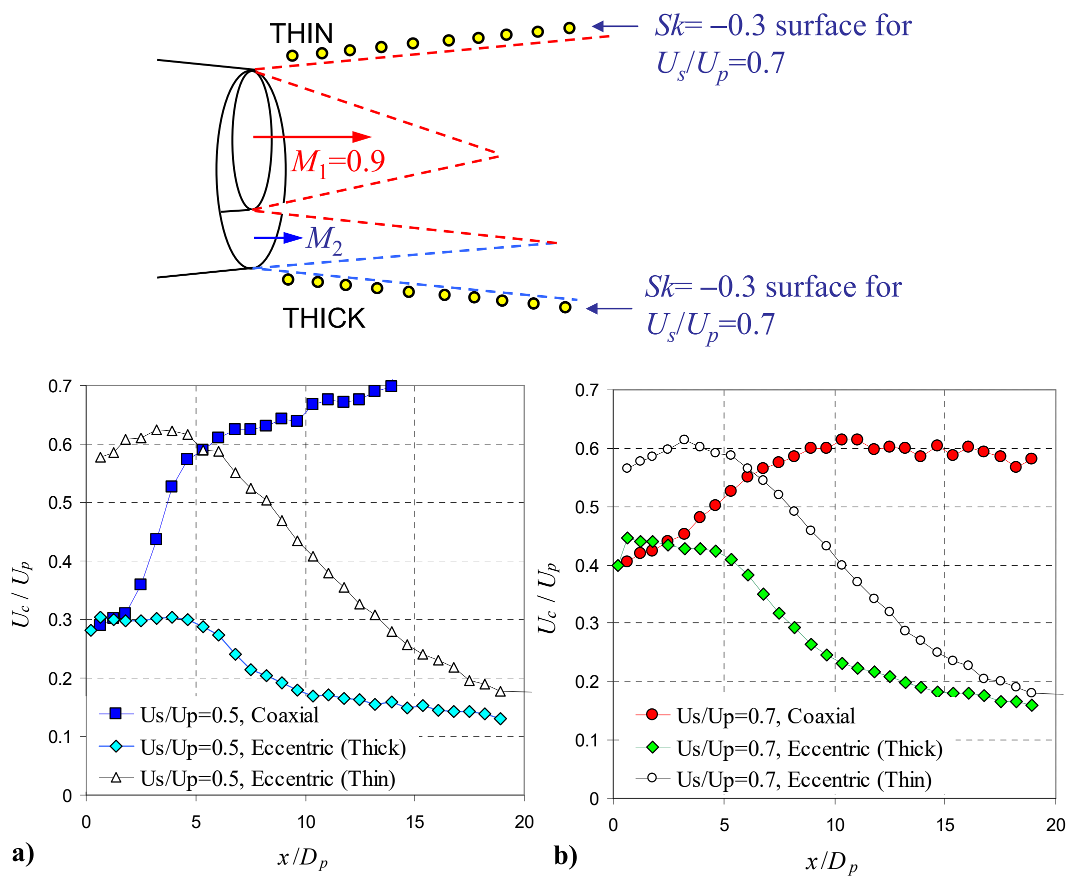

Figure 10. Convective velocity distribution in coaxial and eccentric jets with a) $U_s/U_p = 0.5$ and b) $U_s/U_p = 0.7$.

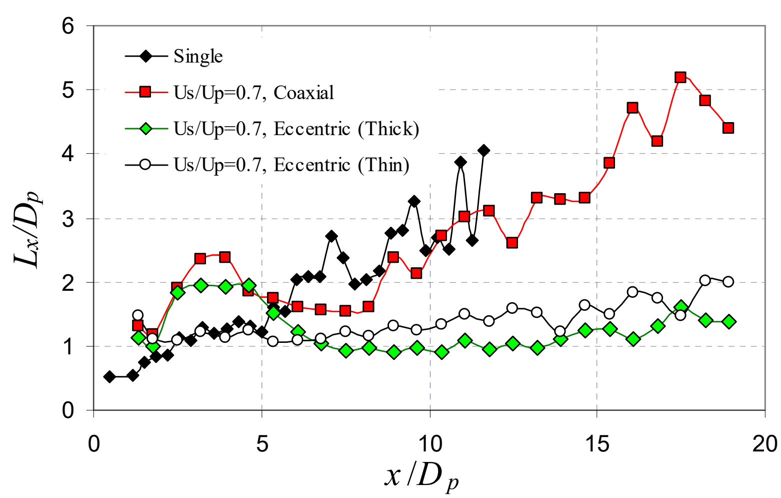

Figure 11. Distribution of the axial correlation scale L_x.

F. Azimuthal Coherence

At a fixed axial station on the radiator surface, we denote $S_{\phi_1,\phi_2}(\omega)$ the cross-spectral density at azimuthal angles ϕ_1 and ϕ_2. The azimuthal coherence is defined as

$$\gamma^2(\phi, \Delta\phi, \omega) = \frac{|S_{\phi,\phi+\Delta\phi}(\omega)|^2}{S_{\phi,\phi}(\omega)\ S_{\phi+\Delta\phi,\phi+\Delta\phi}(\omega)} \tag{10}$$

For axisymmetric jets, $\gamma^2 = \gamma^2(\Delta\phi, \omega)$ and the azimuthal angle ϕ is arbitrary in Eq. 10. For asymmetric jets, however, the azimuthal coherence is a function of the reference azimuthal angle.

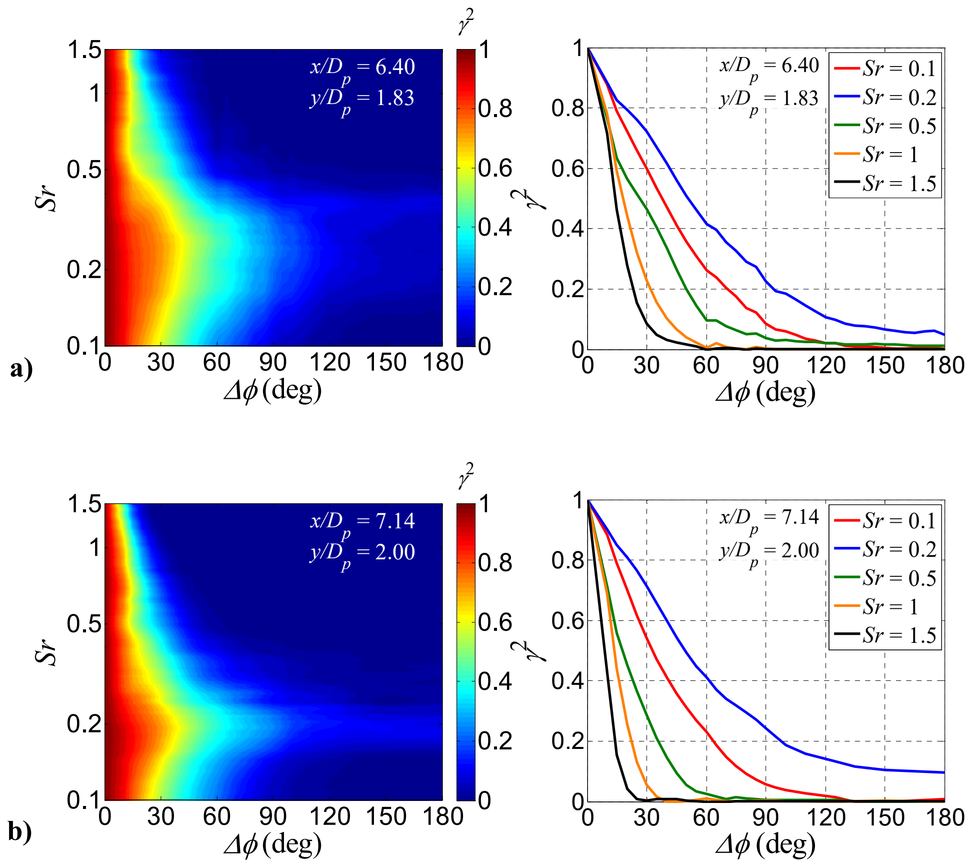

Figure 12. Azimuthal coherence for: a) single-stream jet at $x/D_p = 6.4$; and b) coaxial jet with $U_s/U_p = 0.7$ at $x/D_p = 7.1$.

Figure 12 presents azimuthal coherence measurements for the single-stream jet at $x/D_p = 6.4$ and the coaxial jet with $U_s/U_p = 0.7$ at $x/D_p = 7.1$. The results are presented as contour maps of γ^2 versus Sr and $\Delta\phi$, and as line plots of γ^2 versus $\Delta\phi$ for different Strouhal numbers. The trends for the single and coaxial jets are quite similar. The strongest coherence is observed at $Sr \approx 0.2$. The coherence becomes very weak for Strouhal numbers exceeding about 0.5. Interestingly, the coherence also weakens, but at a lower rate, for very low Strouhal numbers. While at $Sr \approx 0.2$ there is some level of coherence all around the jet, for $Sr \gtrsim 0.5$ the coherence drops to zero at a finite separation angle. For example, at $Sr = 1$ the coherence becomes zero at $\Delta\phi = 60°$ for the single-stream jet and at $\Delta\phi = 35°$ for the coaxial jet. This indicates that at Strouhal numbers on the order of one or higher, which are highly relevant to aircraft noise, the noise source has very limited azimuthal extent. Similar results were noted in the LES correlations of Ref. 10.

For the eccentric jet, the statistics become non-stationary with azimuthal angle and the concept of coherence according to Eq. 10 can break down, especially for large azimuthal separation. Therefore, we restrict ourselves to small separation $\Delta\phi = \pm 20^\circ$ and examine the dependence of the coherence on the reference angle ϕ_{ref}, with $\phi_{\text{ref}} = 0^\circ$ defining the downward vertical. Figure 13 plots the coherence versus Strouhal number for the eccentric jet at $U_s/U_p = 0.7$ and $x/D_p = 8.9$. The reference angle takes the values $\phi_{\text{ref}} = 0^\circ$, 90°, and 180°. The results are compared to the coaxial jet at the same velocity ratio and same axial station. At $\phi_{\text{ref}} = 0^\circ$ (thick side of the secondary flow) the coherence is very weak and drops to zero for $S_r \gtrsim 0.3$. This is in line with the weak axial correlation scale seen in Fig. 11. Since the reference point is on the symmetry plane, the results for $\Delta\phi = \pm 20^\circ$ coincide. Moving the reference angle to $\phi_{\text{ref}} = 90^\circ$, we observe a large difference between the coherence at $\Delta\phi = -20^\circ$ (towards the thick side) and $\Delta\phi = +20^\circ$ (towards the thin side). The coherence toward the thick side is weak, while it is strong towards the thin side. Clearly the statistics there are highly non-stationary with azimuthal angle. At $\phi_{\text{ref}} = 180^\circ$ the coherence is strongest, but not as strong as in the coaxial case. Again, this correlates with the reduced axial correlation on the thin side of the eccentric jet seen in Fig. 11.

It should be kept in mind that the coherence measurements for the eccentric jet were not conducted exactly on its radiator surface, as the geometry of this surface is complex and difficult to map out. Some of the quantitative aspects of the coherence plots in Fig. 13 could be affected by this departure. Nevertheless, it is believed that the qualitative trends are valid and capture important features of the very near pressure field of offset-stream jets.

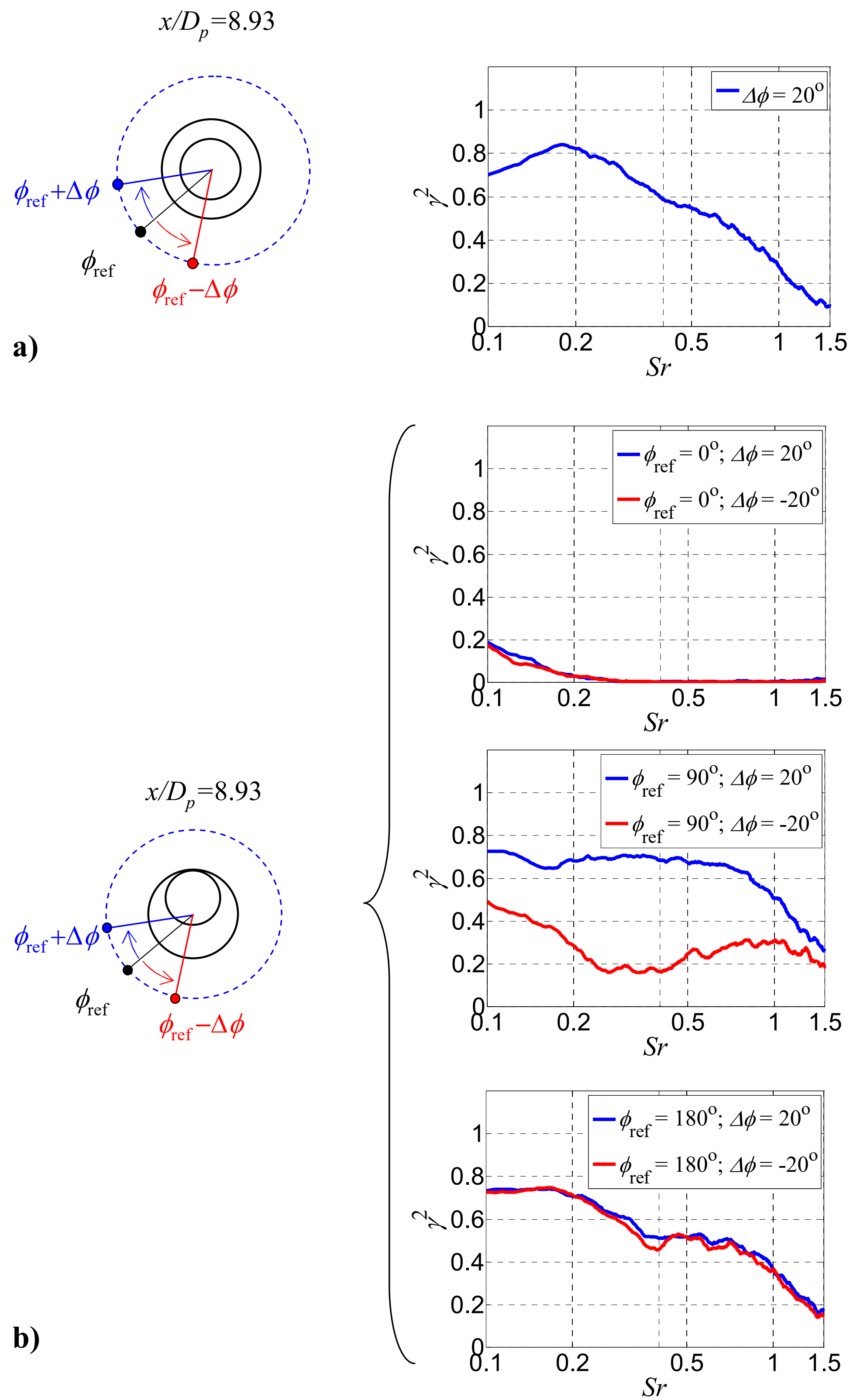

Figure 13. Azimuthal coherence for separation $\Delta\phi = \pm 20^{\circ}$ and various reference angles for: a) coaxial jet at $U_s/U_p = 0.7$; and b) eccentric jet at $U_s/U_p = 0.7$. $\phi_{\mathbf{ref}}$ is defined with respect to the downward vertical.

V. Concluding Remarks

The experimental results of this paper represent an important step towards the development of low-order, surface models of the jet noise source in single- and multi-stream jets. The model is synthesized from partial fields on a "radiator" surface at the boundary between the inner rotational field and the outer irrorational field. This formulation enables computation of the radiated and scattered fields using propagation techniques such as the boundary element method. Use of piezo-resistive transducers as substitutes for microphones enabled the measurement of pressure statistics very close to the edge of single- and dual-stream jets, the latter in coaxial and eccentric configurations.

The very near field pressure measurements indicate that the rotationa/irrotational boundary is characterized by negative skewness of the pressure field, leading to a convenient criterion for defining the radiator surface. Space-time correlations of the pressure fluctuation on the radiator surface yielded the distribution of convective velocity U_c of the partial fields. In coaxial jets, the outer flow effectively silences the eddies of the primary shear layer in the vicinity of the nozzle exit. This is manifested as a large drop in U_c in the initial region of the jet. Offsetting the nozzles prolongs the low-U_c region on the side of the thickened secondary flow. The resulting reduction in radiation efficiency is deemed the primary reason for the noise benefit of eccentric jets. Measurements of the axial and azimuthal correlation scales indicate significant reduction of those scales on the thickened side of the eccentric jets. For the single-stream and coaxial jets, the azimuthal coherence is strongest near Strouhal number 0.2 and reduces rapidly with increasing frequency. At Strouhal numbers above 0.5, the coherence has very limited azimuthal extent, indicating that the partial fields are highly localized circumferentially.

Acknowledgment

We acknowledge the support by NASA Cooperative Agreement NNX14AR98A, monitored by Dr. James Bridges.

References

[1] Ho, C., "Near Field Pressure Fluctuations in a Circular Jet," NASA CR-179847, Nov. 1985.

[2] Zaman, K., "Flow Field and Near and Far Sound Field of a Subsonic Jet," *Journal of Sound and Vibration*, Vol. 106, No. 1, 1986, pp. 1–16.

[3] Avital, E. J., Sandham, N. D., and Luo, K. H., "Mach Wave Radiation by Mixing Layers. Part I: Analysis of the Sound Field," *Theoretical and Computational Fluid Dynamics*, Vol. 12, 1998, pp. 73–90.

[4] Morris, P., "A Note on Noise Generation by Large Scale Turbulent Structures in Subsonic and Supersonic Jets," *International Journal of Aeroacoustics*, Vol. 8, No. 4, 2009, pp. 301–316.

[5] Reba, R., Narayanan, S., and Colonius, T., "Wave-Packet Models for Large-Scale Mixing Noise," *International Journal of Aeroacoustics*, Vol. 9, 2010, pp. 533–558.

[6] Papamoschou, D., "Wavepacket Modeling of the Jet Noise Source," AIAA 2011-2835, June 2011.

[7] Jordan, P. and Colonius, T., "Wave Packets and Turbulent Jet Noise," *Annual Review of Fluid Mechanics*, Vol. 45, 2013, pp. 173–195.

[8] Baqui, Y. B., Agarwal, A., and Cavalieri, A. V. G., "A Coherence-Matched Linear Model for Subsonic Jet Noise," AIAA 2014-2758, Jun 2014.

[9] Papamoschou, D., Xiong, J., and Liu, F., "Reduction of Radiation Efficiency in High-Speed Jets," AIAA 2014-2619, June 2014.

[10] Papamoschou, D., Xiong, J., and Liu, F., "Towards a Low-Cost Wavepacket Model of the Jet Noise Source," AIAA 2015-1006, Jan. 2015.

[11] Papamoschou, D. and Debiasi, M., "Directional Suppression of Noise from a High-Speed Jet," *AIAA Journal*, Vol. 39, No. 3, 2001, pp. 380–387.

[12]Brown, C., Bridges, J., and Henderson, B., "Offset-Stream Technology Test - Summary of Results," AIAA 2007-3664, January 2007.

[13]Huff, D. and Henderson, B., "The Aeroacoustics of Offset Three-Stream Jets for Future Commercial Supersonic Aircraft," AIAA 2016-2992, June 2016.

[14]Papamoschou, D., Phong, V., Xiong, J., and Liu, F., "Quiet Nozzle Concepts for Three-Stream Jets," AIAA 2016-0523, Jan. 2016.

[15]Papamoschou, D., "Noise Suppression in Moderate-Speed Multistream Jets," AIAA 2002-2557, June 2002.

[16]Papamoschou, D., "New Method for Jet Noise Reduction in Turbofan Engines," *AIAA Journal*, Vol. 42, No. 11, 2004, pp. 2245–2253.

[17]Papamoschou, D. and Rostamimonjezi, S., "Effect of Velocity Ratio on Noise Source Distribution of Coaxial Jets," *AIAA Journal*, Vol. 48, No. 7, 2010, pp. 1504–1512.

[18]Doty, M. and McLaughlin, D., "Space-Time Correlation Measurement of High-Speed Axisymmetric Jets Using Optical Deflectometry," *Experiments in Fluids*, Vol. 28, March 2005, pp. 415–425.

[19]Morris, P. and Zaman, K., "Velocity Measurements in Jets with Application to Jet Noise," *Journal of Sound and Vibration*, Vol. 329, 2010, pp. 394–414.